Excitations and relaxation dynamics in multiferroic GeV_4S_8 studied by terahertz and dielectric spectroscopy

S. Reschke,[1] Zhe Wang,[1,*] F. Mayr,[1] E. Ruff,[1] P. Lunkenheimer,[1] V. Tsurkan,[1,2] and A. Loidl[1,†]

[1]*Experimental Physics V, Center for Electronic Correlations and Magnetism, Institute of Physics, University of Augsburg, 86135 Augsburg, Germany*

[2]*Institute of Applied Physics, Academy of Sciences of Moldova, MD-2028 Chisinau, Republic of Moldova*

(Received 19 May 2017; revised manuscript received 14 September 2017; published 16 October 2017)

We report on THz time-domain spectroscopy on multiferroic GeV_4S_8, which undergoes orbital ordering at a Jahn-Teller transition at 30.5 K and exhibits antiferromagnetic order below 14.6 K. The THz experiments are complemented by dielectric experiments at audio and radio frequencies. We identify a low-lying excitation close to 0.5 THz, which is only weakly temperature dependent and probably corresponds to a molecular excitation within the electronic level scheme of the V_4 clusters. In addition, we detect complex temperature-dependent behavior of a low-lying phononic excitation, closely linked to the onset of orbitally driven ferroelectricity. In the high-temperature cubic phase, which is paramagnetic and orbitally disordered, this excitation is of relaxational character becomes an overdamped Lorentzian mode in the orbitally ordered phase below the Jahn-Teller transition, and finally appears as well-defined phonon excitation in the antiferromagnetic state. Abrupt changes in the real and imaginary parts of the complex dielectric permittivity show that orbital ordering appears via a structural phase transition with strong first-order character and that the onset of antiferromagnetic order is accompanied by significant structural changes, which are of first-order character, too. Dielectric spectroscopy documents that at low frequencies, significant dipolar relaxations are present in the orbitally ordered, paramagnetic phase only. In contrast to the closely related GaV_4S_8, this relaxation dynamics that most likely mirrors coupled orbital and polar fluctuations does not seem to be related to the dynamic processes detected in the THz regime.

DOI: 10.1103/PhysRevB.96.144418

I. INTRODUCTION

The cluster compound GeV_4S_8 belongs to the family of lacunar spinels AM_4X_8 (A = Ga and Ge; M = V, Mo, Nb, and Ta; X = S and Se). The structure of lacunar spinels is built by weakly linked cubane $(M_4X_4)^{n+}$ and tetrahedral $(AX_4)^{n-}$ clusters, which are arranged in a fcc-type network [1–3]. Figure 1 illustrates this sodium-chloride structure composed of $(V_4S_4)^{4+}$ and $(GeS_4)^{4-}$ molecular entities. The shorter and longer vanadium bonds, within and in between the cubane clusters, favor the formation of molecular bonds within and prevent metallic bonding between the clusters. The cubane clusters are characterized by a unique electronic distribution, with well-defined total spin of the strongly bonded M_4 molecule. In many cases, the cluster orbitals are only partly occupied, leaving unpaired electrons in the highest, often degenerate electronic levels. As a consequence, many of the lacunar spinels are Jahn-Teller (JT) active and, as a function of temperature, the orbital degeneracy is lifted by a symmetry-lowering structural phase transition [4,5]. In lacunar spinels, a variety of interesting phenomena, such as pressure-induced superconductivity [6,7], substantial resistive switching [8–10], and metal-to-insulator transitions [11,12], were identified. They also belong to the rather rare class of materials, where orbital order, which is established at the JT transition, induces ferroelectricity [13,14]. Ferroelectricity driven by orbital order is a fascinating topic in modern condensed-matter physics [15–17]. Furthermore, in GaV_4S_8 and GV_4Se_8, complex low-temperature, low-field phase diagrams have been reported, including cycloidal, skyrmion, and spin-polarized ferromagnetic phases [18–21]. In these compounds, in addition to the significant ferroelectric polarization, which arises at the JT transition, all magnetic phases reveal spin-driven excess polarizations, including skyrmions, which are dressed with ferroelectric polarization [14].

Many lacunar spinels exhibit a sequence of phase transitions, which is known from some canonical multiferroics. Quite crudely, multiferroics can be subdivided into two groups [22,23]: In type-I multiferroics, ferroelectricity and magnetism are of different origins and, in many of these compounds, the ferroelectric ordering temperature is significantly higher than the magnetic one. Perovskite-derived $BiFeO_3$ belongs to this class of materials [24]. A special group of multiferroics are materials in which ferroelectricity is induced by charge order [23]. Magnetite is an illuminating example of this class of systems [25]. In type-II multiferroics, ferroelectricity is driven by spin order, such as in ferroelectric perovskite manganites [26], and spin and polar order occur at the same temperature. The lacunar spinels have to be classified as type-I multiferroics, where ferroelectricity is driven by orbital order and magnetism has a different origin and appears at significantly lower temperatures. However, in some systems, such as in GaV_4S_8, additional ferroelectric polarization is induced at the onset of magnetic order [14], which makes these compounds mixed type-I and type-II systems.

Here we report on terahertz (THz) optical and dielectric properties of the semiconducting lacunar spinel GeV_4S_8, which is a multiferroic compound with orbital-order-driven ferroelectricity coexisting with the antiferromagnetic (AFM) ground state. In this compound, the highest occupied cluster orbital of the V_4 molecules is triply degenerate and filled with

*Present address: Helmholtz-Zentrum Dresden Rossendorf, Bautzner Landstraße 400, 01328 Dresden, Germany.

†alois.loidl@physik.uni-augsburg.de

 ©2017 American Physical Society

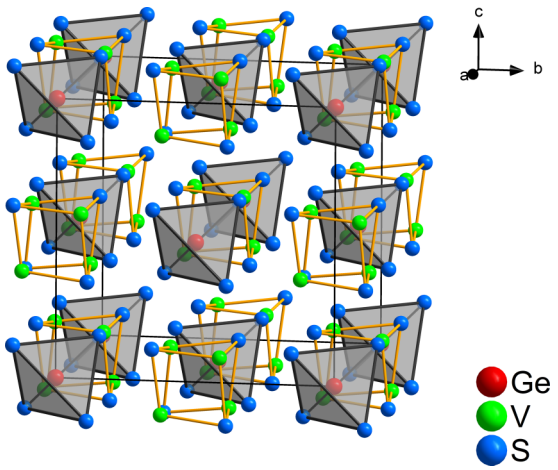

FIG. 1. Crystallographic structure of the high-temperature phase of the lacunar spinel GeV_4S_8. Yellow bars indicate the V_4S_4 cubane clusters and the GeS_4 tetrahedra are light-gray colored. The solid lines constituting a cube indicate the fcc high-temperature structure of the lacunar spinels. a–c correspond to the crystallographic axes of the cubic cell.

two unpaired electrons constituting a total spin $S = 1$ [3,5]. In GeV_4S_8, the orbital degeneracy is lifted by a JT-like structural phase transition from the cubic $F\bar{4}3m$ room-temperature phase to the orthorhombic phase with $Imm2$ symmetry at $T_{JT} \approx 30-33$ K [4,13,27,28]. Orbitally induced ferroelectricity in GeV_4S_8 has been clearly identified [13,28] and some experimental evidence has been provided that this structural phase transition consists of two subsequent transitions, which are very close in temperature. In Ref. [28], it was speculated that this sequence of phase transitions could signal the decoupling of ionic and electronic degrees of freedom in establishing ferroelectric order. THz and dielectric spectroscopy is well suited to unravel the coupled orbital and dipolar dynamics. Wang *et al.* [29] systematically studied the relaxation dynamics at the JT transition of the skyrmion host GaV_4S_8. By combining THz and dielectric experiments at radio frequencies, they found an interesting noncanonical behavior of the polar relaxation dynamics of this material at the orbital-order-driven ferroelectric transition. One aim of the present work is to check for similar behavior in the closely related Ge compound.

However, GeV_4S_8 represents a spin $S = 1$ system and the resulting JT distortions in the germanium and the gallium compounds are fundamentally different. While in GaV_4S_8 ($S = 1/2$) the V_4 tetrahedra are elongated along one out of the four crystallographic $\langle 111 \rangle$ directions, in GeV_4S_8, the V_4 tetrahedral units distort with one short and one long vanadium bond on adjacent sites [27]. At lower temperatures, in GeV_4S_8, antiferromagnetic order is established at $T_N = 13-18$ K [4,5,13,27,28]. In distinct contrast, the skyrmion host GaV_4S_8 is close to ferromagnetic order and, in zero external magnetic field, reveals cycloidal spin order below 12.7 K [19]. It has to be noted that a THz investigation on ceramic samples of GeV_4S_8, in a somewhat limited temperature and frequency range when compared to the present study, was very recently published by Warren *et al.* [30]. Preliminary dielectric results have been published in Refs. [13,28]. However, in this work, we mainly focus on the relaxation dynamics. Detailed studies of the temperature dependence of the phonon response of GaV_4S_8 and GeV_4S_8 have been presented in Refs. [31–33]. While the authors of these studies report on distinct anomalies in the temperature dependence of eigenfrequencies and damping at the JT transition, no indications of a clear soft-phonon behavior, as expected in canonical ferroelectrics, were found. References [31,33,34] provide detailed first-principles calculations of phonon properties for these lacunar spinels.

II. EXPERIMENTAL DETAILS

Experimental details concerning sample preparation and characterization of GeV_4S_8 have been given in Ref. [28]. The single crystals, which were used in the THz experiments of this work, have a structural JT transition close to $T_{JT} = 30.5$ K, where long-range orbital order is induced, and they exhibit antiferromagnetic order below $T_N = 14.6$ K. Both transitions are strongly of first order [28]. The magnetic susceptibility and magnetization can best be described by localized moments of the V_4 molecules with spin $S = 1$ and strong antiferromagnetic exchange. The single crystals used in these experiments have been oriented using Laue diffraction. For transmission THz measurements, a GeV_4S_8 single crystal of size $4 \times 4\,mm^2$ was prepared, with a thickness of 0.65 mm. The time-domain THz transmission experiments using a TPS Spectra 3000 spectrometer (TeraView Ltd.) were performed perpendicular to the (111) plane for frequencies from approximately 0.2–3 THz in a He-flow cryostat (Oxford Instruments) between liquid-helium and room temperature. In these terahertz time-domain experiments, THz pulses are emitted and detected using repetition rates of 80 MHz. Electric fields of the THz signals are recorded as a function of time delay for the sample and a reference (an empty aperture). The time-domain signals are then Fourier transformed to obtain transmission and phase shift in the frequency domain. By modeling the sample as a dielectric slab, the complex refractive index, $n = n_1 - in_2$, the complex dielectric constant, $\varepsilon = \varepsilon_1 - i\varepsilon_2$, or the complex electrical conductivity, $\sigma = i\omega\varepsilon = \sigma_1 - i\sigma_2$, can be directly calculated. For details of the spectroscopic principles of THz experiments, see Refs. [35]. In the present experiments, at low frequencies (<0.5 THz), the experiments suffer from the limited sample size and from multiple reflections in the cryostat windows and sample. At high frequencies (>3 THz), the precision is limited by the decreasing intensity of the THz source. This will be discussed later in more detail. The dielectric properties of GeV_4S_8 were measured at audio and radio frequencies for temperatures between 4 and 300 K. These experiments in the frequency range from 1 Hz to 10 MHz were performed with a frequency-response analyzer (Novocontrol Alpha-Analyzer). In the dielectric experiments, we used platelet-shaped single crystals of approximately $4\,mm^2$ cross section and 0.4 mm thickness, in most cases with the electric field applied along the crystallographic $\langle 111 \rangle$ direction. For this purpose, silver-paint contacts were applied to opposite sides of the crystals.

III. RESULTS AND DISCUSSION

A. THz spectroscopy

At THz frequencies, the complex dielectric permittivity $\varepsilon = \varepsilon_1 - i\varepsilon_2$ was determined in the temperature range between

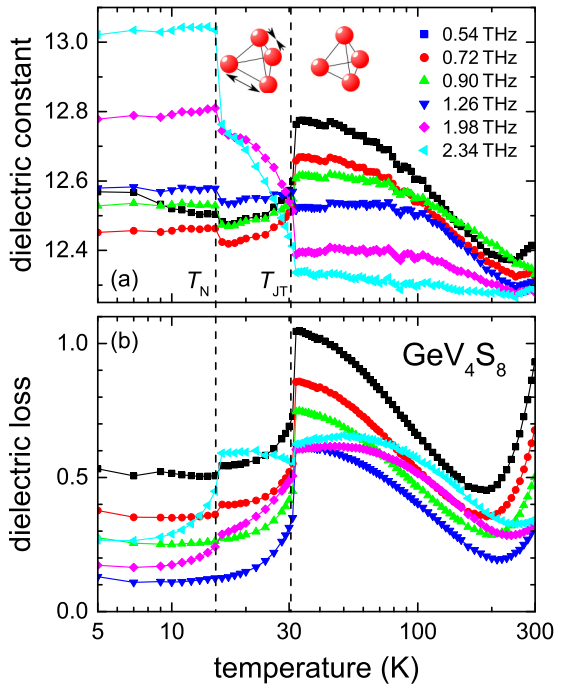

FIG. 2. Semilogarithmic plot of the temperature dependence of the complex dielectric permittivity of GeV_4S_8. Data are shown between 5 K and room temperature for selected frequencies between 0.54 and 2.34 THz. (a),(b) The dielectric constant ε_1 and loss ε_2, respectively. The dashed vertical lines indicate the JT transition at $T_{JT} = 30.5$ K and the onset of AFM order at $T_N = 14.6$ K. The solid lines connect the data points. It is not straightforward to calculate error bars of the complex permittivity shown in (a) and (b). In this respect, the best measure certainly is the temperature-dependent scatter of the data. In (a) we provide a schematic view of the vanadium tetrahedron, which is regular in the high-temperature phase and strongly distorted in the orbitally ordered phase below the Jahn-Teller transition. The arrows indicate the local distortions (see text).

5 and 300 K. Figure 2 shows the temperature dependence of the real and imaginary parts of ε for a series of frequencies between 0.5 and 2.3 THz. Both the AFM ($T_N = 14.6$ K) and the structural transition ($T_{JT} = 30.5$ K) can be identified via significant changes in the temperature and frequency dependences of the dielectric constant ε_1 and loss ε_2. The abrupt changes of these quantities at the phase boundaries document the first-order character of both transitions. The transition temperatures are in perfect agreement with the corresponding values reported in Ref. [28]. Both ε_1 and ε_2 exhibit significant frequency dependences in all three temperature regimes, namely, in the magnetically ordered, the orbitally ordered, and the cubic high-temperature phase, which is in contrast to the results in GaV_4S_8 [29], where all dispersion effects were almost completely suppressed below the JT transition. The dielectric constant ε_1 in GeV_4S_8 is about 12–13, somewhat lower than in the related gallium compound with $\varepsilon \approx 15$ [29]. It is also worth mentioning that from a recent far-infrared study [32], the dielectric constant at THz frequencies has been determined to be 13.2, in good agreement with the present result.

Figure 2 reveals strong dispersion effects at all temperatures. However, there is no straightforward interpretation of these dielectric THz data. In the paramagnetic and orbitally disordered phase, for 1.98 and 2.34 THz, the temperature dependence of the dielectric loss ε_2 exhibits a well-developed maximum close to 50 K, which slightly shifts to lower temperatures on decreasing frequencies. This signals, at least in this temperature range, relaxational behavior of the dipolar degrees of freedom at the JT transition, similar to the observations in GaV_4S_8 [29]. However, temperature and frequency dependence at lower temperatures indicates that the relaxation dynamics must be more complex. The increase of the dielectric loss towards high temperatures above 200 K most likely signals the importance of dc conductivity contributions at elevated temperatures. These conductivity contributions at high temperatures will not be discussed in the following. Below the transitions, for most frequencies, ε_2 is observed to decrease with decreasing temperature. This decrease may signify the low-frequency flanks of relaxation or other excitation peaks, whose characteristic times (and, thus, peak temperatures) become shifted at the transitions, preventing the detection of the peak temperature, but clear statements are not possible based on the data shown in Fig. 2 alone.

To arrive at a more detailed description of the dynamic processes in GeV_4S_8, Fig. 3 shows the frequency dependences of the real [Fig. 3(a)] and imaginary [Fig. 3(b)] parts of the dielectric permittivity ε, for selected temperatures between 5 and 300 K. In the frequency dependences of both quantities, the phase boundaries close to 15 and 31 K can be easily identified: At these temperatures, the THz response dramatically changes, obviously forced by significant (first-order) structural changes, in accord with Fig. 2. Turning first to the imaginary part [Fig. 3(b)], in the complete temperature regime, ε_2 exhibits an increase towards low frequencies. At the lowest temperatures, this increase indicates an excitation just at the lower edge of

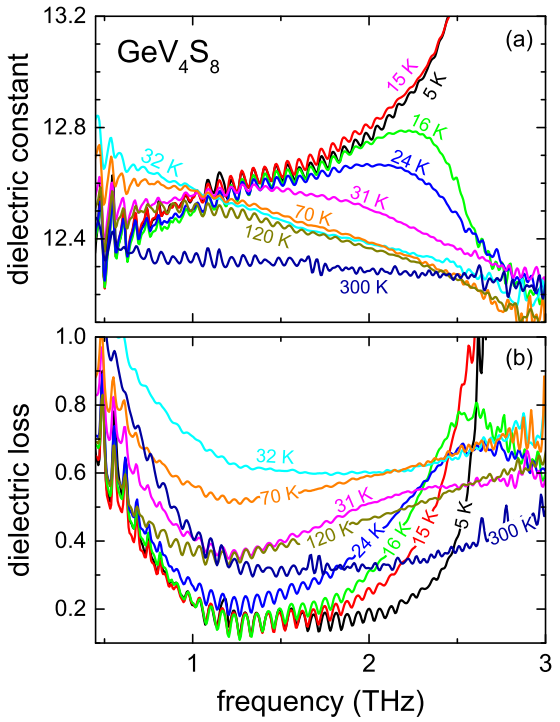

FIG. 3. Frequency dependence of the (a) dielectric constant ε_1 and (b) dielectric loss ε_2 of GeV_4S_8 between 0.5 and 3 THz for selected temperatures between 5 and 300 K.

the probed frequency range. When assuming a Lorentzian-type excitation, the decrease of the dielectric constant ε_1 towards low frequencies observed at low temperatures seems to be compatible with this interpretation. Indeed, a well-defined excitation close to 0.3 THz between 8 and 24 K has been reported by Warren *et al.* [30]. The eigenfrequency of this excitation was found to exhibit almost no temperature dependence, even when crossing the antiferromagnetic phase transition, and has been interpreted as phononlike excitation in the orbitally ordered phase. We tend to ascribe this excitation to a characteristic mode of the molecular V_4 clusters. We would like to recall that a threefold-degenerate level forms the highest occupied orbital of these clusters [3]. It could well be that slight local distortions induce a lifting of this degeneracy. The eigenfrequency of approximately 0.3 THz seems to be too low for a canonical phononlike excitation. Assuming specific symmetry conditions of the high-temperature paraelectric phase, infrared-active phonon modes in GeV_4S_8 are not expected below 4.5 THz, while in the orbitally ordered phase, the lowest eigenfrequency was predicted to occur at 2 THz [33]. Hlinka *et al.* [31] calculated the eigenfrequencies of phonon excitations in the cubic high-temperature phase of GaV_4S_8 and found the lowest infrared active mode at 3.4 THz.

When we follow the temperature evolution of this low-lying excitation, as documented in Fig. 3(b), on increasing temperatures the increase in ε_2 becomes weaker, seems to be weakest close to 120 K, but then increases again on further increasing temperatures. In the high-temperature regime ($T >$ 120 K), this increase in ε_2 certainly stems from dc conductivity contributions and can be described by a frequency dependence $\varepsilon_{2,\mathrm{dc}} \propto \sigma_{\mathrm{dc}}/\omega$.

At the lowest temperatures, in the antiferromagnetically ordered phase, both ε_1 and ε_2 show a strong increase towards higher frequencies. This can naturally be explained assuming a relatively strong Lorentzian-like excitation close to 3 THz, most probably a phonon excitation of the low-temperature antiferromagnetic phase. Focusing on the frequency dependence of the real and imaginary parts of the dielectric permittivity, this phonon excitation abruptly becomes heavily damped for $T > T_{\mathrm{N}}$, in the paramagnetic but orbitally ordered phase. This is impressingly documented in both frames of Fig. 3, when comparing dielectric constant and dielectric loss measured at 5 and 15 K, with values derived at 16, 24, and 31 K. It seems natural to assume that just above T_{N}, orbital fluctuations set in, which strongly couple to this phonon mode. Despite strong damping, the excitations in the orbitally ordered phase still are of the Lorentzian type with well-defined eigenfrequency. This is best seen by the decrease of the dielectric constant below the maximum in $\varepsilon_1(T)$. However, with further increasing temperatures ($T >$ 31 K), this excitation becomes even more strongly damped and appears as a relaxational mode above the JT transition in the high-temperature cubic and orbitally disordered phase. In this temperature regime, the coupling of orbital fluctuations to the phonon excitation seems to be even stronger and the THz response probably has to be interpreted in terms of a dynamic JT effect [33]. It is unclear at present if a small phonon contribution remains at high frequencies close to 3 THz in the high-temperature cubic phase.

To describe the frequency-dependent permittivity data in GeV_4S_8 as documented in Fig. 3, we choose the following approach:

$$\varepsilon = \sum_{j=1}^{3} \frac{\Delta\varepsilon_j \omega_{0,j}^2}{\omega_{0,j}^2 - \omega^2 - i\gamma_j\omega} + \frac{\Delta\varepsilon_D}{1 + (i\omega\tau)^{1-\alpha}} - i\frac{\sigma_{\mathrm{dc}}}{\varepsilon_0\omega} + \varepsilon_\infty. \tag{1}$$

The first term of Eq. (1) describes a sum of Lorentzian oscillators. Here, $\Delta\varepsilon$ is the dielectric strength of each mode, ω_0 is its (transverse) eigenfrequency, and γ is the damping. The single oscillators are denoted with the indices $j = 1$, 2, and 3, respectively. The second term in Eq. (1) corresponds to a broadened Debye relaxation with the relaxation strength $\Delta\varepsilon_{\mathrm{D}}$, the mean relaxation timeτ, and the width parameter α. If the width parameter is zero, this term corresponds to a monodispersive Debye relaxation. For nonzero values of α, the relaxation becomes symmetrically broadened and corresponds to a Cole-Cole distribution of relaxation times [36]. For the analysis of the THz spectra, the width parameter was set to 0, while for the dielectric results, the Cole-Cole distribution has been used. In the case of the THz results, this relaxation term is only included for temperatures $T > T_{\mathrm{JT}}$ and replaces the Lorentzian contribution of the high-frequency phonon. The third term describes a contribution from dc conductivity σ_{dc}. Conductivity contributions are relevant only for temperatures $T >$ 150 K and are not further considered here.

Three Lorentz oscillators [first term in Eq. (1) with $j = 1, 2,$ and 3] are needed to describe the low-frequency excitations in the magnetically ordered phase ($T < T_{\mathrm{N}}$). These include the low- and high-frequency modes discussed above, appearing close to 0.5 and 2.8 THz. As will be documented below, a further excitation at about 1.65 THz, which only exists in the orbitally ordered phases, has to be taken into account to arrive at a good description of the experimental results at the lowest temperatures. Three Lorentzian-type oscillators are also needed to describe the spectra in the paramagnetic orbitally ordered phase ($T_{\mathrm{N}} < T < T_{\mathrm{JT}}$), with a very low dipolar weight close to experimental uncertainty of the middle excitation at about 1.65 THz. This is in accord with the results by Warren *et al.* [30] and this observation discards this excitation as antiferromagnetic resonance. In the high-temperature cubic phase ($T > T_{\mathrm{JT}}$), only a single Lorentzian excitation (at low frequencies) plus a relaxational mode are necessary to describe the THz spectra. A further very weak mode, close to 0.6 THz, was detected in Ref. [30] in the AFM phase. We were not able to locate this excitation in our spectra.

To document the difficulties in fitting these spectra, Fig. 4 shows the fit results in the AFM phase at 13 K and in the orbitally ordered but paramagnetic phase at 20 K. In these fits, we deconvoluted the spectra to make the contributions of the three Lorentzian-type excitations more clear. The difficulties result from the fact that the lowest and highest excitations in the AFM phase are close to the limit of the THz spectral range. At low frequencies, the aperture is of a size comparable to the wavelength, while at high frequencies, the intensity of the THz radiation is already very low. In addition, although the phonon mode close to 3 THz is so strong that the effective transmission becomes zero and hence the peak maximum cannot be measured, the signal is recovered beyond this phonon mode. In the orbitally ordered phase, below the

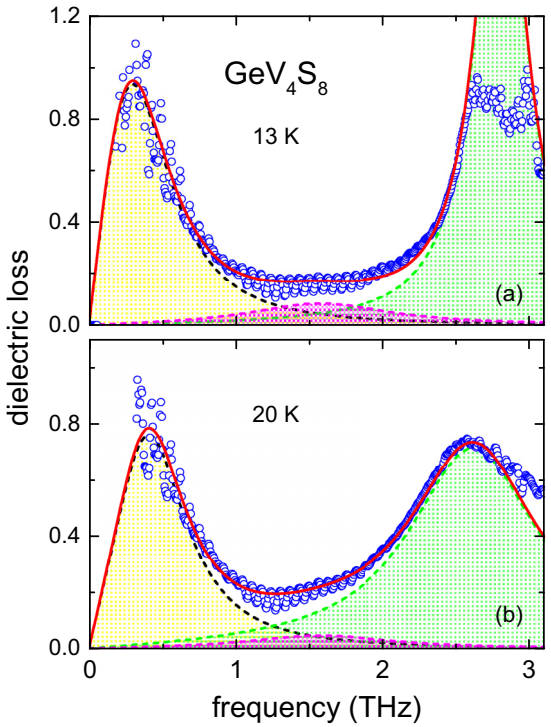

FIG. 4. Representative fits of the frequency dependence of the dielectric loss ε_2 of GeV_4S_8 (symbols) at (a) 13 K and (b) 20 K. The (red) solid line represents the total fit, while the dashed lines show the fit results decomposed into three Lorentzian contributions, which have been colored for better visibility. In the peak center, the Lorentzian line close to 3 THz has a transmission close to zero and, in the analysis, in this regime is set to a minimal value (see text).

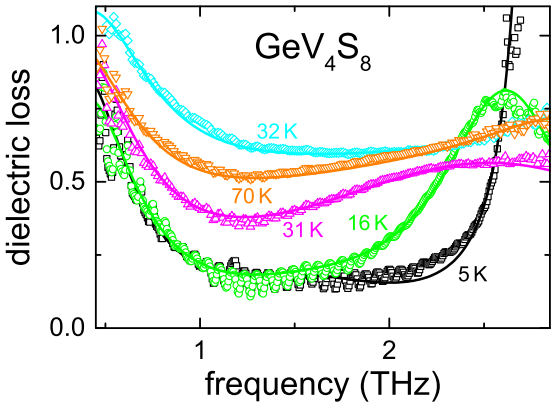

FIG. 5. Frequency dependence of the dielectric loss ε_2 of GeV_4S_8 (symbols) and corresponding fits using Eq. (1) (solid lines). Spectra are shown for a series of representative temperatures in the AFM and orbitally ordered phase (5 K), in the paramagnetic and orbitally ordered phase (16 and 31 K), as well as in the cubic high-temperature phase (32 and 70 K). Due to the very weak intensity of the excitation close to 1.65 THz, which exists in the orbitally ordered phases only, its eigenfrequency and damping, which are rather well defined at low temperatures, have been fixed in the fitting procedure (see text and Fig. 6).

Jahn-Teller transition, we identified increasing intensity in the intermediate-frequency range, which is well defined at low temperatures but becomes very weak when approaching the structural phase transition. Despite these challenges, we were able to arrive at a consistent description of all our results. In Figs. 4 and 5, we only show the frequency dependence of the dielectric loss. However, one should have in mind that we always also analyzed the real part of the dielectric constant. These fits are not shown, but provide further evidence of the correctness and reliability of the fit results.

To document the evolution of these modes when passing through the magnetic and structural phase transition, Fig. 5 shows typical results of the fits to the imaginary part of the dielectric permittivity for selected temperatures (lines). Here the main focus is on intermediate frequencies to show that the well-defined phonon mode close to 3 THz in the AFM phase evolves into a strongly broadened excitation in the paramagnetic and orbitally ordered phase, and finally into a purely relaxational mode in the high-temperature cubic phase. Reasonable agreements of fit and experimental curves are achieved in all phases, namely, in the magnetically ordered (5 K), in the paramagnetic and orbitally ordered (16 and 31 K), as well as in the high-temperature cubic (32 and 70 K) phases. The significant excitation close to 0.5 THz shows only little temperature dependence. It is slightly shifted and moderately broadened, but can be identified as a well-defined excitation in the complete temperature range shown in Fig. 5. Hence, it also seems to exist even in the high-temperature cubic phase. The temperature evolution towards room temperature can hardly be followed, as on increasing temperatures the dc conductivity contribution becomes more important and masks this excitation [see Fig. 3(b)]. In the magnetically ordered phase, a well-defined phonon mode close to 2.8 THz dominates the spectrum. As discussed above, at the transition to the paramagnetic phase, the damping of this phonon excitation abruptly increases and this excitation considerably broadens on further increasing temperatures. However, up to the JT transition at 31 K, despite the unusual broadening, this excitation remains to be of the Lorentzian type, i.e., with a well-defined eigenfrequency. However, in the high-temperature cubic phase, with the loss of orbital order, this excitation becomes fully overdamped and can now be described using a single Debye relaxation, only characterized by a mean relaxation time. The significant change of character of this excitation from a Lorentzian to relaxational type is best documented comparing the frequency dependence of the dielectric loss at 31 and 32 K (Fig. 5).

Figure 6 shows the temperature dependence of the parameters of the three excitations that dominate the THz response of GeV_4S_8 below 100 K. At higher temperatures, the spectra are governed by contributions from dc conductivity and the analysis of low-lying excitations becomes rather unreliable. The lowest excitation [Figs. 6(a)–6(c)] appears close to 0.5 THz in the AFM phase. As detailed above, the fitting procedure was not straightforward. We were only able to measure the high-frequency flank of the lowest mode with high precision. The mode at 1.7 THz is of vanishing intensity and, in the AFM phase, the high-frequency mode is only well defined below the peak maximum. Hence, we partly fixed some of the parameter, which can be well identified in Fig. 6 (e.g., eigenfrequency of the low-frequency mode in the orbitally ordered but paramagnetic phase [Fig. 6(a)],

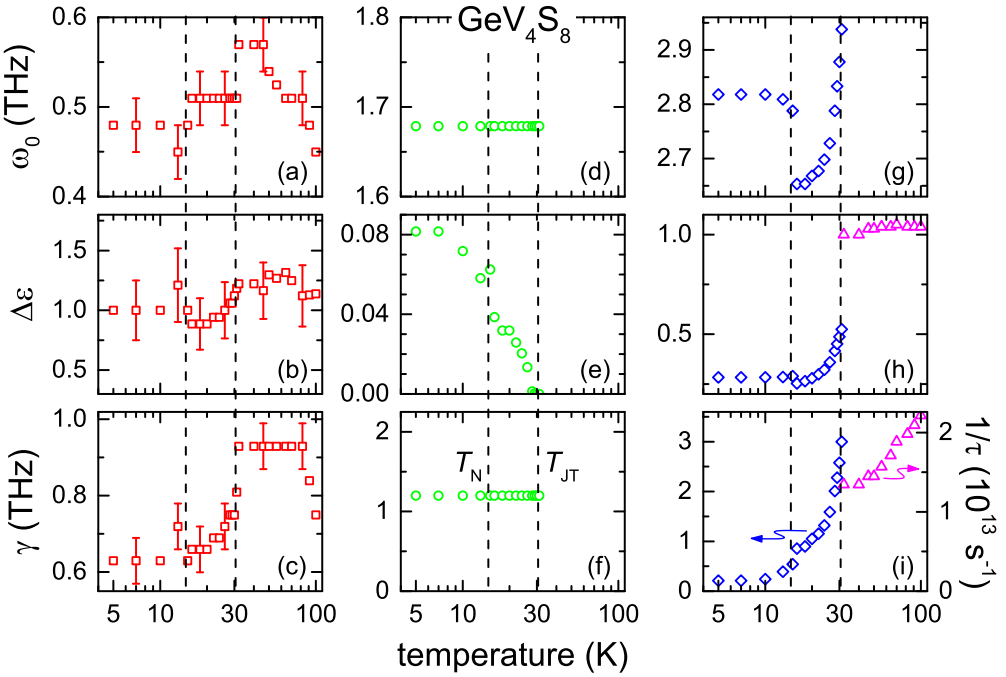

FIG. 6. Temperature dependence of the fitting parameters of the THz response in GeV_4S_8 for the three modes as documented in Figs. 4 and 5 for temperatures $T < 100$ K. (a)–(c) show the parametrization of the low-frequency excitation: (a) eigenfrequency, (b) dielectric strength, and (c) damping. (d)–(f) document the temperature evolution of the parameters for the weak resonance close to 1.65 THz: (d) eigenfrequency, (e) dielectric strength, and (f) damping. (g)–(i) show the parameters observed for the Lorentzian-like phonon mode for $T < T_{JT}$: (g) eigenfrequency, (h) dielectric strength, and (i) damping. For $T > T_{JT}$, a parameterization in terms of a Debye relaxation was used: (h) relaxation strength and (i) mean inverse relaxation time (right axis).

partly the damping of this mode in the high-temperature phase [Fig. 6(c)], eigenfrequency of the excitation close to 1.7 THz [Fig. 6(d)], as well as damping of this mode [Fig. 6(f)]). The eigenfrequency shown in Fig. 6(a) exhibits an upward jump to about 0.6 THz just above the JT transition and then decreases on further increasing temperatures. The mode strength [Fig. 6(b)] remains essentially constant up to 100 K within the experimental uncertainties. The damping shows a continuous increase with temperature in the paramagnetic, orbitally ordered phase [Fig. 6(c)]. As mentioned above, the eigenfrequency seems to be too low for a canonical phonon mode. Most probably, this excitation corresponds to a collective mode belonging to the V_4 cluster molecules.

Overall, our results are in reasonable agreement with those derived by Warren *et al.* [30]. As discussed earlier, these authors investigated the frequency regime from 0.2 up to 1.4 THz on polycrystalline samples. In this regime, they identified a strong excitation close to 0.3 THz, which they related to the V_4 cluster dynamics. A rather weak excitation was found close to 1.2 THz, which increases in intensity below T_N. In our study, both excitations appear at somewhat higher energies, namely, at 0.48 and 1.68 THz. It is unclear if this fact results from different excitation geometries or from the use of different samples. The latter appears with the onset of orbital order and increases continuously down to the lowest temperatures. There is a minor upward step at the onset of magnetic order, indicating some coupling to spin degrees of freedom. Warren *et al.* [30] identified a very weak excitation close to 0.6 THz, which cannot be identified in our experiments.

The excitation close to 1.7 THz [Figs. 6(d)–6(f)] seems to exist in the orbitally ordered phases only. As it survives the transition into the paramagnetic phase, a magnetic dipole transition probably can be excluded. Due to its very low dipolar strength, for the fits the eigenfrequency and damping had to be fixed. This excitation continuously loses dipolar weight when approaching the JT transition [Fig. 6(e)] and is completely absent in the cubic high-temperature phase. Hence, it seems to be correlated with the onset of orbital order. The fact that its intensity continuously decreases towards the structural phase transition makes orbital excitations within an excitation scheme due to lifted orbital degeneracy likely. Detailed model calculations will be necessary to arrive at finite conclusions.

Finally, Figs. 6(g)–6(i) show the parameters of the strong and dominating phonon mode observed in the AFM phase close to 2.8 THz. In the magnetically ordered phase, this phonon mode remains rather constant, with moderately increasing damping on increasing temperatures [Fig. 6(i)]. At the AFM-to-paramagnetic phase transition, this mode abruptly jumps to lower eigenfrequencies [Fig. 6(g)], but then eigenfrequency and oscillator strength [Fig. 6(h)] continuously increase on further increasing temperatures. Most remarkable, its damping increases by a factor of 4 when the temperature is raised from the AFM to the structural phase transition. Finally, in the high-temperature cubic phase, this mode loses its oscillatory character and transforms into a purely relaxational mode.

It seems interesting to compare the results as documented in Fig. 6 with phonon frequencies calculated by *ab initio* calculations [33] or observed in canonical infrared reflectivity

experiments [32,33]. In these experiments, no phonon modes were observed below approximately 9 THz, either in the orbitally ordered or in the high-temperature phases [32,33]. Following *ab initio* calculations, in the orbitally ordered and ferroelectric state, a relatively strong mode is expected close to 2 THz [33], which indeed could correspond to the mode observed close to 1.68 THz in the course of this work [Fig. 6(d)]. This mode appears below the Jahn-Teller transition and does not exist in the high-temperature phase. The strong mode, which at the lowest temperatures is close to 2.8 THz, broadens considerably on increasing temperatures and becomes purely relaxational for temperatures above the Jahn-Teller transition. The purely relaxational character of this excitation could signal a dynamic Jahn-Teller effect with accompanying dynamic distortions. It is interesting to note that Cannucia *et al.* [33] speculated about a lower-symmetric high-temperature phase, mainly guided by the disagreement between calculated and observed phonon eigenfrequencies. This observation was interpreted by a dynamical Jahn-Teller distortion model. Indeed, a dynamic Jahn-Teller effect governing the high-temperature phase could be the origin of the relaxational mode, which evolves out of the phonon excitation close to 2.8 THz in the AFM phase. However, much more experimental and theoretical work is needed to strengthen this conclusion.

Finally, it seems almost impossible to arrive at definite conclusions concerning the low-temperature mode close to 0.5 THz [Fig. 6(a)]. This mode exists at least up to 100 K. In our experiments, the analysis at higher temperatures is hampered by increasing dc conductivity contributions. This mode could be an orbital excitation or an intrinsic excitation from the $(M_4X_4)^{4+}$ molecules. Guided by its temperature dependence, Warren *et al.* [30] speculated that this mode originates from the V_4 cluster dynamics.

B. Dielectric results

Preliminary results of dielectric measurements at radio and audio frequencies have been previously reported [13], partly also by our group [28]. Here we focus on the dynamics of relaxational processes and try to compare the results with those derived by THz spectroscopy discussed above. Figure 7 shows the dielectric constant $\varepsilon'(T)$ of GeV_4S_8 measured at frequencies between 178 Hz and 316 kHz along the crystallographic ⟨111⟩ direction for temperatures from 10 to 50 K. This temperature regime covers the onset of orbital order at 30.5 K and the phase transition into long-range antiferromagnetic order at 14.6 K. The shown data were measured on heating and, for clarity, the dielectric data are shown on a semilogarithmic plot. Both phase transitions are indicated by abrupt steplike changes of the dielectric constant, which amount to more than 100 at low frequencies. These drastic changes of ε' are not due to Maxwell-Wagner contributions from the surface or from domain walls or grain boundaries [37], but certainly result from abrupt changes in the dipolar relaxation dynamics. The temperature dependence of the dielectric constant reveals a domelike enhancement in the temperature regime between the two phase transitions. On cooling, the temperature dependence of the dielectric constant is of similar shape (not shown), but exhibits significantly lower values of $\varepsilon'(T)$ in between the

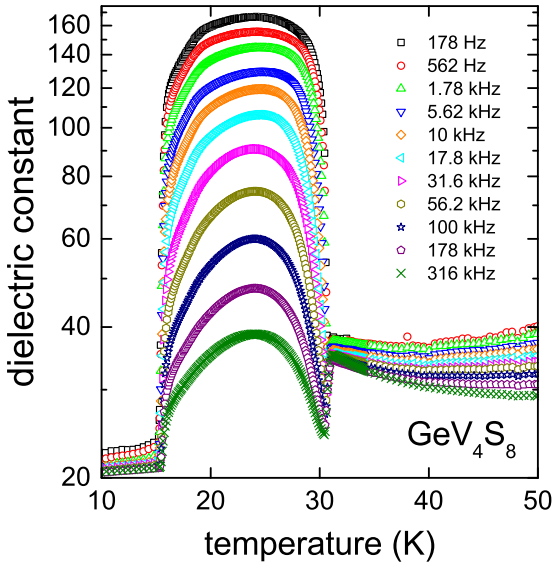

FIG. 7. Temperature dependence of the real part of the permittivity of GeV_4S_8 measured along the crystallographic ⟨111⟩ direction at frequencies between 178 Hz and 316 kHz under heating on a semilogarithmic plot.

structural and magnetic phase transitions. Singh *et al.* [13] have reported very similar behavior of the temperature dependence of the dielectric constant. We would like to pinpoint the fact that in Ref. [28], the V-shaped minimum in $\varepsilon'(T)$, just below the structural phase transition, was interpreted as a possible fingerprint of a separation of electronic (charge distribution) and ionic displacements in the ferroelectric ordering process.

These highly unusual temperature and frequency dependences of the dielectric constant look drastically different from the dispersion effects observed in the THz regime [see Fig. 2(a)]. At first glance, this dielectric response at audio and radio frequencies may be explained by assuming that dipolar relaxations, which dominate the dielectric response in the THz regime in the orbitally disordered phase, are shifted to much lower frequencies at the onset of orbital order, but become fully suppressed again at the magnetic phase transition. An extreme slowing down of the relaxation dynamics when orbital order sets in also characterizes the orbitally driven ferroelectric transition in GaV_4S_8 [29]. In this compound, a single dipolar relaxation dominates the THz response in the high-temperature phase, while in the orbitally ordered phase it shows up at radio frequencies and persists down to the lowest temperatures. This behavior was discussed in terms of an order-disorder-type polar transition that is of strongly first order [29]. However, already a first inspection of Figs. 3 and 7 makes clear that the dipolar dynamics at the structural and magnetic phase transitions in GeV_4S_8 is more complex: For this material, various dynamic processes are observed in the THz regime for all temperatures (Figs. 2–4). At audio and radio frequencies, a significant dipolar relaxation process can only be identified in the orbitally ordered paramagnetic phase (Fig. 7). Just as for GaV_4S_8, in GeV_4S_8 we indeed also observe a relaxational process above the JT transition at THz frequencies. However, in contrast to the Ga system [29], it seems unlikely that this THz relaxation reflects the coupled polar and orbital

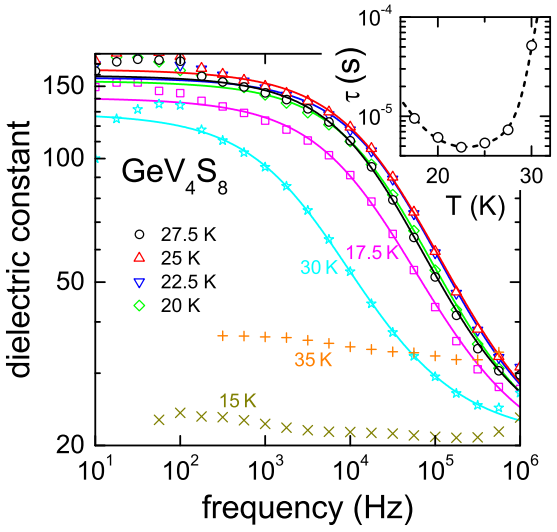

FIG. 8. Dielectric constant vs frequency in GeV_4S_8 for a series of temperatures between 15 and 35 K on a double-logarithmic plot. The solid lines represent results of polydispersive Cole-Cole fits as described in the text. The inset shows the temperature dependence of the mean dipolar relaxation time as determined from these fits. The dashed line in the inset is drawn to guide the eye.

dynamics associated with the ferroelectric transition and shifts to the radio-frequency regime below the JT transition. As discussed above, below T_{JT}, it instead remains located in the THz regime and changes its character from relaxational to resonancelike. Thus, the relaxational dynamics that appears at low frequencies in the polar-ordered paramagnetic phase, dominating the dielectric properties at audio/radio frequencies (Fig. 7), does not seem to be simply connected with the relaxation dynamics in the THz regime, which changes its nature and character but is observable in all phases.

To affirm the relaxational character of the observed dispersion at audio and radio frequencies and to get an estimate of the temperature evolution of the mean relaxation times, Fig. 8 shows the frequency dependence of the real part of the dielectric permittivity for selected temperatures in the regime between the two phase transitions. Just above the orbital-order transition (35 K) and just below the AFM transition (15 K), the dielectric constant is low, nearly frequency independent, and a significant time scale of a possible relaxation can hardly be determined. However, strong dispersion effects appear between 17.5 and 30 K, just in the orbitally ordered and paramagnetic phase, with a steplike decrease of the dielectric constant from a plateau with high values at low frequencies to low values at high frequencies. This indeed is the typical signature of a relaxational process. The data can reasonably well be fitted assuming a polydispersive relaxation.

To fit the dielectric data, we took Eq. (1), neglecting the Lorentzian contributions [first term in Eq. (1)] and allowing for a symmetrically broadened polydispersive Cole-Cole relaxation, with a nonzero width parameter α. The relevant fit parameters are the dielectric strength $\Delta\varepsilon_D$, the mean relaxation time τ, the high-frequency dielectric constant ε_∞, and the width parameter α, which takes a symmetric broadening of the relaxation due to structural inhomogeneities into account. The

TABLE I. Parameters of the fits of the frequency dependence of the dielectric constant in the orbitally ordered and paramagnetic phase between 17.5 and 30 K, as documented by solid lines in Fig. 8.

T (K)	$\Delta\varepsilon_D$	τ (s)	ε_∞
17.5	122.8	9.54E-06	17.8
20	136.5	6.10E-06	18.0
22.5	139.6	4.87E-06	17.9
25	148.0	5.37E-06	17.0
27.5	140.4	7.27E-06	19.0
30	108.2	5.17E-05	20.8

fit results are shown as solid lines in Fig. 8 and the temperature dependence of the relevant fit parameters are given in Table I. In all these fits, the width parameter of the symmetrically broadened distribution has been kept fixed at 0.4. The relaxation strength is maximum close to 25 K and explains the broad hump visible in Fig. 7. At these temperatures, the relaxation times are minimal. The infinite dielectric constant is enhanced when compared to the values observed in the THz regime (Figs. 2 and 3). In fitting the real part of the dielectric constant, dc conductivity contributions play no role. The mean relaxation times τ, which were derived from these fits, are plotted in the inset of Fig. 8. They slow down towards the onset of magnetic order at low temperatures and towards the structural phase transition at high temperatures. Between the two phase transitions, the relaxation times are of the order of μs, several decades slower than the relaxation times in the ns range reported for GaV_4S_8 below T_{JT} [29]. This further supports the notion that in contrast to the latter compound, for GeV_4S_8 there is no connection of the relaxational responses detected by the dielectric and THz experiments.

It seems useful to discuss the precision and possible error bars of the quantities listed in Table I and partly shown in the inset of Fig. 8, which have been determined from fits of the frequency dependence of the dielectric constants. The values of the mean relaxation times are determined by the points of inflection of the frequency-dependent steps of the dielectric constant plotted in Fig. 8. These values are rather well defined and possible error bars are of the order of 5%, roughly corresponding to the size of the symbols in the inset of Fig. 8. The values of the high-frequency dielectric constant ε_∞ are determined by the high-frequency plateau of the dielectric constants, which is not fully reached in the present experiments. Consequently, error bars can reach values of the order of 20%. The dielectric strength $\Delta\varepsilon_D$ is determined by the step heights of the frequency-dependent dielectric constant, with rather well-defined low-frequency and ill-defined high-frequency values and possible error bars that will be of the order of 15%.

For canonical order-disorder ferroelectrics, by dielectric spectroscopy usually a relaxation process is detected arising from fluctuations of the same dipolar degrees of freedom that lead to polar order [38]. Its temperature-dependent relaxation time rises at the ferroelectric transition. Thus, the detected increase of $\tau(T)$ when approaching the transitions from within the orbitally ordered paramagnetic phase, documented in the inset of Fig. 8, may well reflect such a behavior. As in GeV_4S_8, just as for GaV_4S_8 [29], polar and orbital degrees

of freedom seem to be closely coupled, and this relaxation process most likely simultaneously mirrors the polar and orbital dynamics, located in the audio- and radio-frequency range for temperatures between the two transitions.

IV. CONCLUSIONS

In this work, by utilizing THz and audio- to radio-wave dielectric spectroscopy, we have investigated the polar relaxational dynamics in GeV_4S_8 associated with the orbital-order-driven ferroelectric transition. Our aim was to check for similar noncanonical behavior as found for the order-disorder scenario of the ferroelectric transition in GaV_4S_8. The main conclusion is that the relaxation dynamics in the germanium compound is completely different when compared to the gallium lacunar spinel. This probably results from the fact that the JT transition in the $S = 1$ germanium system is of a different nature and induces a different low-temperature structure, finally resulting in low-temperature antiferromagnetic spin order.

In the THz study, we detected a number of low-lying excitations: Close to 0.5 THz, we identified a Lorentzian-type excitation with weak temperature dependence of eigenfrequency, damping, and dielectric strength. This excitation probably corresponds to a transition within the split orbital ground state of the vanadium molecules in the low-symmetry low-temperature phases. As there are still some ambiguities concerning the low-temperature structure of the AFM phase and as no realistic calculations of the orbital scheme of the molecular V_4 entities are available, we cannot arrive at finite conclusions. We identify a further weak excitation close to 1.7 THz, whose dipolar strength goes to zero, when approaching the JT transition. This low-energy excitation could correspond to a phononlike excitation as proposed by Warren *et al.* [30]. In the ferroelectric *Imm*2 phase, the lowest IR active phonon frequency with reasonable strength was predicted at 2 THz [33].

In addition, in the low-temperature magnetically ordered phase, a phononlike excitation close to 2.8 THz was most unexpectedly identified, which reveals a very unusual temperature dependence of both eigenfrequency and damping. The damping heavily increases (by more than a factor of 10) in the paramagnetic and orbitally ordered phase when approaching the JT transition. Ultimately, in the high-temperature orbitally disordered phase, this excitation becomes heavily overdamped and can be described as broad Debye-like relaxation.

Finally, we have also presented detailed dielectric spectroscopy at audio and radio frequencies. We find a relaxation process with significant dielectric dispersion only in the orbitally ordered and paramagnetic phase. It most likely mirrors the coupled orbital and polar dynamics that cause the ferroelectric order. The relaxation times are in the μs regime and slow down when approaching the structural as well as the magnetic transition. In marked contrast to observations in GaV_4S_8 [29], there does not seem to be a close connection between this relaxation dynamics and the excitations present in the THz regime.

ACKNOWLEDGMENTS

We acknowledge stimulating discussions with I. Kézsmárki and partial support by the Deutsche Forschungsgemeinschaft (DFG) via the Transregional Collaborative Research Center TRR 80 "From Electronic Correlations to Functionality" (Augsburg, Munich, Stuttgart).

[1] H. Barz, Mat. Res. Bull. **8**, 983 (1973).
[2] J. M. Vandenberg and D. Brasen, J. Solid State Chem. **14**, 203 (1975).
[3] D. Johrendt, Z. Anorg. Allg. Chem. **624**, 952 (1998).
[4] H. Chudo, C. Michioka, H. Nakamura, and Y. Yoshimura, Physica B **378**, 1150 (2006).
[5] H. Müller, W. Kockelmann, and D. Johrendt, Chem. Mater. **18**, 2174 (2006).
[6] M. M. Abd-Elmeguid, B. Ni, D. I. Khomskii, R. Pocha, D. Johrendt, X. Wang, and K. Syassen, Phys. Rev. Lett. **93**, 126403 (2004).
[7] R. Pocha, D. Johrendt, B. Ni, and M. M. Abd-Elmeguid, J. Am. Chem. Soc. **127**, 8732 (2005).
[8] L. Cario, C. Vaju, B. Corraze, V. Guiot, and E. Janod, Adv. Mater. **22**, 5193 (2010).
[9] V. Guiot, L. Cario, E. Janod, B. Corraze, V. Ta Phuoc, M. Rozenberg, P. Stoliar, T. Cren, and D. Roditchev, Nat. Commun. **4**, 1722 (2013).
[10] V. Dubost, T. Cren, C. Vaju, L. Cario, B. Corraze, E. Janod, F. Debontridder, and D. Roditchev, Nano Lett. **13**, 3648 (2013).
[11] V. Ta Phuoc, C. Vaju, B. Corraze, R. Sopracase, A. Perucchi, C. Marini, P. Postorino, M. Chligui, S. Lupi, E. Janod, and L. Cario, Phys. Rev. Lett. **110**, 037401 (2013).
[12] A. Camjayi, C. Acha, R. Weht, M. G. Rodriguez, B. Corraze, E. Janod, L. Cario, and M. J. Rozenberg, Phys. Rev. Lett. **113**, 086404 (2014).
[13] K. Singh, C. Simon, E. Cannuccia, M.-B. Lepetit, B. Corraze, E. Janod, and L. Cario, Phys. Rev. Lett. **113**, 137602 (2014).
[14] E. Ruff, S. Widmann, P. Lunkenheimer, V. Tsurkan, S. Bordács, I. Kézsmárki, and A. Loidl, Sci. Adv. **1**, e1500916 (2015).
[15] P. Barone, K. Yamauchi, and S. Picozzi, Phys. Rev. B **92**, 014116 (2015).
[16] K. Yamauchi and P. Barone, J. Phys. Condens. Matter. **26**, 103201 (2014).
[17] B. Keimer, Nat. Mater. **5**, 933 (2006).
[18] I. Kézsmárki, S. Bordács, P. Milde, E. Neuber, L. M. Eng, J. S. White, H. M. Ronnow, C. D. Dewhurst, M. Mochizuki, K. Yanai, H. Nakamura, D. Ehlers, V. Tsurkan, and A. Loidl, Nat. Mater. **14**, 1116 (2015).
[19] S. Widmann, E. Ruff, A. Günther, H.-A. Krug von Nidda, P. Lunkenheimer, V. Tsurkan, S. Bordács, I. Kézsmárki, and A. Loidl, Philos. Mag. (2016), doi:10.1080/14786435.2016.1253885.
[20] Y. Fujima, N. Abe, Y. Tokunaga, and T. Arima, Phys. Rev. B **95**, 180410(R) (2017).

[21] S. Bordács, A. Butykai, B. G. Szigeti, J. S. White, R. Cubitt, A. O. Leonov, S. Widmann, D. Ehlers, H.-A. Krug von Nidda, V. Tsurkan, A. Loidl, and I. Kézsmárki, Sci. Rep. **7**, 7584 (2017).
[22] D. I. Khomskii, J. Magn. Magn. Mater. **306**, 1 (2006).
[23] J. van den Brink and D. I. Khomskii, J. Phys. Condens. Matter **20**, 434217 (2008).
[24] J. Lu, A. Günther, F. Schrettle, F. Mayr, S. Krohns, P. Lunkenheimer, A. Pimenov, V. D. Travkin, A. A. Mukhin, and A. Loidl, Europhys. J. B **75**, 451 (2010).
[25] F. Schrettle, S. Krohns, P. Lunkenheimer, V. A. M. Brabers, and A. Loidl, Phys. Rev. B **83**, 195109 (2011).
[26] T. Kimura, T. Goto, H. Shintal, K. Ishizaka, T. Arima, and Y. Tokura, Nature (London) **426**, 55 (2013).
[27] D. Bichler, V. Zinth, D. Johrendt, O. Heyer, M. K. Forthaus, T. Lorenz, and M. M. Abd-Elmeguid, Phys. Rev. B **77**, 212102 (2008).
[28] S. Widmann, A. Günther, E. Ruff, V. Tsurkan, H.-A. Krug von Nidda, P. Lunkenheimer, and A. Loidl, Phys. Rev. B **94**, 214421 (2016).
[29] Z. Wang, E. Ruff, M. Schmidt, V. Tsurkan, I. Kézsmárki, P. Lunkenheimer, and A. Loidl, Phys. Rev. Lett. **115**, 207601 (2015).
[30] M. T. Warren, G. Pokharel, A. D. Christianson, D. Mandrus, and R. Valdes Aguilar, Phys. Rev. B **96**, 054432 (2017).
[31] J. Hlinka, F. Borodavka, I. Rafalovskyi, Z. Docekalova, J. Pokorny, I. Gregora, V. Tsurkan, H. Nakamura, F. Mayr, C. A. Kuntscher, A. Loidl, S. Bordács, D. Szaller, H.-J. Lee, J. H. Lee, and I. Kézsmárki, Phys. Rev. B **94**, 060104(R) (2016).
[32] S. Reschke, F. Mayr, Zhe Wang, P. Lunkenheimer, Weiwu Li, D. Szaller, S. Bordács, I. Kézsmárki, V. Tsurkan, and A. Loidl, Phys. Rev. B **96**, 144302 (2017).
[33] E. Cannuccia, V. T. Phuoc, B. Brière, L. Cario, E. Janod, B. Corraze, and M. B. Lepetit, J. Phys. Chem. C **121**, 3522 (2017).
[34] K. Xu and H. J. Xiang, Phys. Rev. B **92**, 121112(R) (2015).
[35] B. Gorshunov, A. Volkov, I. Spektor, A. Prokhorov, A. Mukhin, M. Dressel, S. Uchida, and A. Loidl, Int. J. Infrared Millimeter Waves **26**, 1217 (2005).
[36] K. S. Cole and R. H. Cole, J. Chem. Phys. **9**, 341 (1941).
[37] P. Lunkenheimer, V. Bobnar, A. V. Pronin, A. I. Ritus, A. A. Volkov, and A. Loidl, Phys. Rev. B **66**, 052105 (2002).
[38] M. E. Lines and A. M. Glass, *Principles and Application of Ferroelectrics and Related Materials* (Clarendon, Oxford, 1977).